Geometric Analysis for the Size Estimation of Subsurface Delamination in Transient Electromagnetic Response

Tzu-Yang Yu and Burak Boyaci
Department of Civil and Environmental Engineering
University of Massachusetts Lowell
One University Avenue, Lowell, MA 01854, U.S.A.

ABSTRACT

Detection of subsurface defects (e.g., delamination, cracking) using microwave/radar sensors (e.g., ground penetrating radar or GPR) is an important and promising technique for the effective and efficient maintenance of civil infrastructure. In this technique, reflected and scattered electromagnetic signals are typically collected and used for interpreting the size and property of subsurface damages. The objective of this paper is to investigate the feasibility of using finite measurements in the reflected signal for size estimation, through the geometric analysis of waveform. Simulated transient electromagnetic response was generated by finite difference time domain (FDTD) methods in two dimensional domain. A modulated Gaussian impulse at a center frequency of 3.5 GHz was used as the source. Rectangular delaminations with a width ranging from 3.048 cm to 16.256 cm and a thickness of 0.762 cm were considered. The depth of subsurface delamination was also studied. The curvature of reflected waveforms, obtained by three measurements, was used to correlate with the width of subsurface delamination. A relative width parameter was defined and used in the proposed equations for estimating the delamination width with less than 10% error. It is found that the relative width parameter is linearly proportional to the difference in waveform curvature. The proposed approach is potentially applicable to other subsurface defects with different shapes.

Keywords: : Subsurface delamination, geometric analysis, finite difference time domain, ground penetrating radar, transient electromagnetic response

1. INTRODUCTION

Deterioration of civil infrastructure has become a challenging problem in most countries in the world. Progressive and sudden failures of civil infrastructure can result in immediate and long-term catastrophic impact. It is understood that deteriorated infrastructure systems need to be inspected, monitored, rehabilitated, and strengthened before their retirement. In any case, condition assessment techniques (e.g., nondestructive testing/evaluation/inspection) are essential to the effective maintenance of deteriorated civil infrastructure to determine the level of deterioration. Among various nondestructive evaluation (NDE) techniques (e.g., optical, acoustic, thermal, magnetic, electrical, microwave/radar), microwave/radar methods have demonstrated as a promising tool applicable for the surface and subsurface inspection of civil infrastructure systems. Figure 1 shows the data collection scheme and imaging of ground penetrating radar (GPR). Figure 1 shows the data collection scheme in typical GPR operation and the imaging result from a two-dimensional scan (B-scan). The data collection scheme of GRP results in the formation of a series of ridge waves when subsurface anomalies (e.g., pipeline, delamination, landmines) are present. Knowing that the size of subsurface anomalies is proportional to the size of ridge waves, it is of interest to develop a quantitative relationship between anomalies and ridge waves. The objective of this paper is develop a quantitative relationship between subsurface anomalies and measured ridge waves in GPR images using finite different time domain (FDTD) methods. Such information can be useful for the rapid evaluation of subsurface anomalies in the subsurface GPR inspection/assessment of civil infrastructure.

Further author information: (Send correspondence to T.-Y. Yu)
E-mail: Tzuyang_Yu@UML.EDU, Telephone: 1 617 230 7402

Nondestructive Characterization for Composite Materials, Aerospace Engineering, Civil Infrastructure, and Homeland Security 2011, edited by H. Felix Wu, Proc. of SPIE Vol. 7983, 79831J · © 2011 SPIE
CCC code: 0277-786X/11/$18 · doi: 10.1117/12.880558

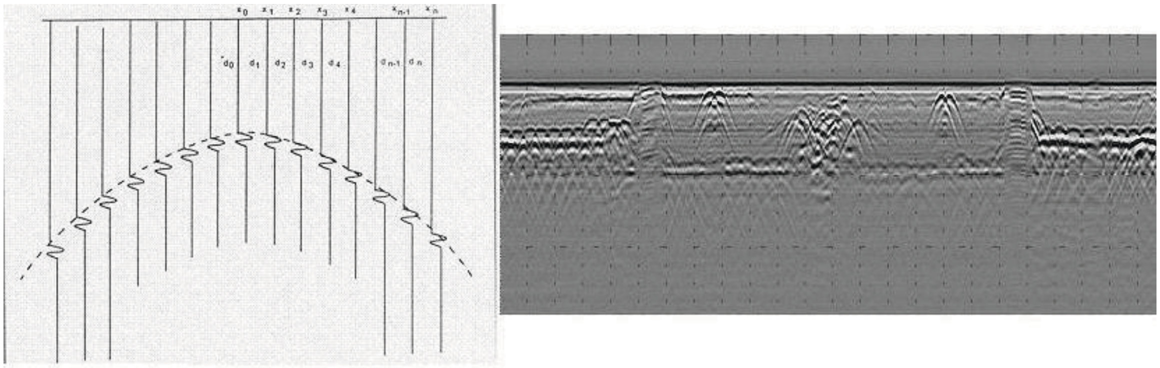

(A) Data collection (B) Typical GPR image from subrusface sensing

Figure 1. GPR data collection scheme and imaging[1]

In the following sections, use of FDTD methods on GPR applications is first reviewed. Research approach (FDTD methods) and designed numerical models are described, followed by simulation results. A quantitative relationship between the characteristic length of subsurface rectangular defects is proposed. Finally, research findings are summarized and discussed.

2. REVIEW OF FDTD ON GPR APPLICATIONS

Simulations of GPR responses using FDTD methods have been reported by various researchers in the past; Liu *et. al.* (2007)[7] used FDTD methods to simulate the tunnel coating quality inspection using GPR. In their model, a concrete layer containing metal wires was laid on rock with two delaminations (one filled with water between the concrete and the 15 rock layers). The dielectric constant and conductivity of the concrete and the rock was assigned to be 6, 0.005 S/m and 5, 0.0001 S/m, respectively. The center frequency of the antenna was 900 MHz, and the excitation source was a Gaussian pulse. Reflection from the delaminations was found to be not clear due to the interference of strong metal wire scattering in the B-scan. However, another simulation model was performed without the presence of the metal wires; the delamination between the concrete and the rock layer was clearly identified in the B-scan.

Zhan *et. al.* (2008)[6] modeled the GPR application on bridge decks using FDTD methods. Both 2D and 3D models of reinforced concrete bridge deck were created to compare the detectibility of the delamination between asphalt and concrete layer and the delamination inside reinforced concrete. The dielectric constants of asphalt and concrete were assumed to be 5 and 9 respectively. A bistatic GPR elevated at 30.6 cm from the asphalt layer was used as an excitation pulse source with 1.0 GHz center frequency to create B-scan images. It was shown that 2D and 3D simulations resulted in approximately the same B-scans for different kinds of defect scenario. Because the bridge deck was relatively uniform in the third dimension and the computational time of 2D simulations were short, it was suggested that 2D simulation is a good approximation for bridge deck models although the accuracy of 3D simulation is superior when the geometry of the model becomes complicated.

Nojavan *et. al.* (2009)[8] simulated the GPR response of reinforced concrete structures using FDTD and used the Born imaging algorithm for damage detection. A reinforced concrete slab, a horizontal crack and a debonding layer between concrete and one of the rebars were modeled in their 2D FDTD simulations. Dielectric constant and conductivity of the concrete was assigned to be 5.3 and 0.05 S/m, respectively. The center wavelength of the excitation signal in concrete was about 1.7 cm. Actuators and the receivers were densely placed on the upper surface of the modeled slab. Images were constructed from the scattered field created by the excitation of each actuator and obtained from each receiver. It was shown that damage geometries can be estimated correctly using the Born imaging algorithm and any components of electromagnetic field (i.e. Ey, Hz, Hx) can be utilized to identify the damage.

Neyrat *et. al.* (2009)[4] used monostatic and multistatic B-scan to simulate the detection of burried objects using GPR. One transmitter emitting a modulated Gaussian impulse with a center frequency of 1.0 GHz and ten receivers employed to detect the buried pipes in heterogeneous medium (dielectric constant assigned as 6). In multistatic B-scan, retiming method was applied by taking the delay between the various receivers into account. The resulting monostatic and retimed multistatic B-scans were compared. It is shown that the B-scan of the latter provides better detectibility than the former. On the other hand, wavefront migration technique is introduced to remove unwanted reflections and hyperbolic reflection characteristics of buried objects from B-scan.

3. RESEARCH APPROACH – FINITE DIFFERENCE TIME DOMAIN METHODS

In this paper, the finite difference time domain (FDTD) methods using Yee's algorithm[3] was chosen for its superior performance and capability of generating the space-time response of electromagnetic (EM) wave propagation and scattering. The central difference scheme is selected for its higher order of accuracy over the forward and backward difference schemes. Introduction to the FDTD methods can be found in the literature.[2]

3.1 Space and Time Discretization

When describing the FDTD models used in computational domain, spatial (Δx, Δy, Δz) and temporal (Δt) increments must be properly defined to ensure numerical/computational stability. Two criteria are applied in the FDTD simulation; the sampling (Nyquist) theorem and the Courant-Friedirchs-Levy (CFL) stability theorem. According to the sampling theorem which is defined by the folding or Nyquist frequency, the necessary sampling rate in time, Δt, is determined by

$$\Delta t < \frac{1}{2 f_{\max}} \tag{1}$$

where $f_{\max}$ is the maximum frequency content (Hz) (Nyquist frequency) that is allowed to ensure the signal can be fully reconstructed at sampling rate Δt.[9] For instance, given a maximum frequency f= 10 GHz, the sampling rate must be less than 5×10^{-11} sec or 5×10^{-2} ns.

The other criterion is adopted to deal with the coupling between Δt and spatial increments (Δx, Δy, Δz) is the Courant-Friedirchs-Levy (CFL) or the Courant stability criterion which is defined by[10]

$$\Delta t < \frac{1}{c\sqrt{\frac{1}{\Delta x} + \frac{1}{\Delta y} + \frac{1}{\Delta z}}} \tag{2}$$

For uniform discretization in three-dimensional problems we have $\Delta t < \frac{\Delta x}{c\sqrt{3}}$, and $\Delta t < \frac{\Delta x}{c\sqrt{2}}$ for two-dimensional problems. Derivation of the CFL stability criterion can be found at Courant *et. al.* (1967).[10] For example, Δt must be less than 3.538×10^{-3} ns for Δx= 0.0015 m. In the FDTD simulation of this paper, $\Delta x = \Delta y = 0.00254$ m (0.254 cm).

3.2 Absorbing Boundary Condition

In the numerical simulation of EM wave propagation and scattering in free space, the use of reflectionless boundaries is necessary in order to simulate the infinite physical environment (open space or free space) in a finite/bounded domain. Such boundary conditions are termed absorbing boundary condition (ABC). Among various types of ABC, the perfectly matched layer (PML) ABC[11] is used. PML ABC is read as

$$\frac{\sigma}{\epsilon_0} = \frac{\sigma^*}{\mu_0} \tag{3}$$

In PML ABC, the effect of enforcing the electric conductivity σ of the ABC medium to satisfy Eq.[3] is equivalent to the creation of a lossless vacuum in the ABC region.

3.3 Incident Signal

In the FDTD simulation of this paper, a modulated Gaussian signal with center frequency at 3.5 GHz was used as the incident signal. Figure 3.3 shows the waveform of the modulated Gaussian signal.

Description of the FDTD models is provided in the following paragraphs.

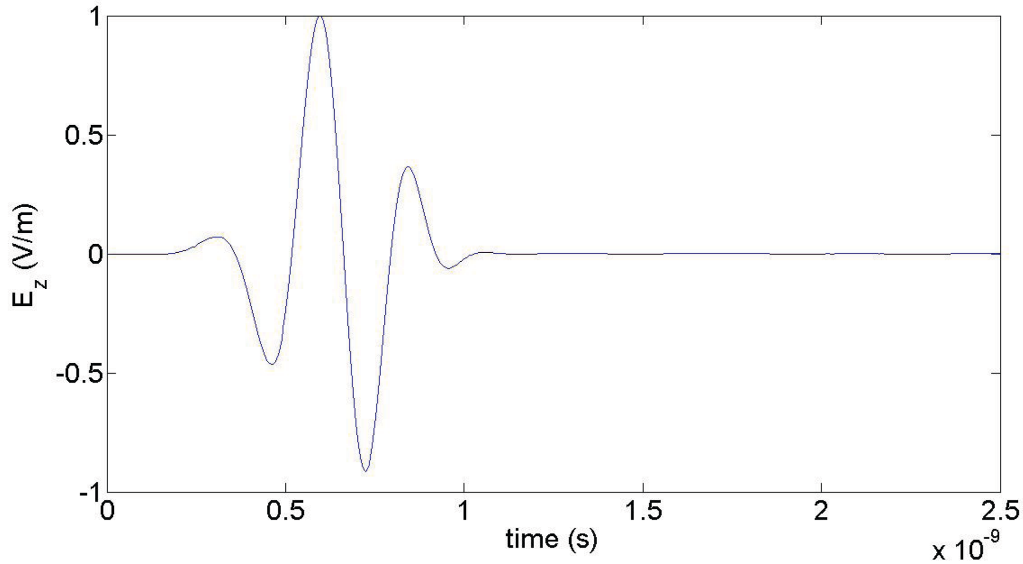

Figure 2. Waveform of the incident GPR signal

4. NUMERICAL MODELS

In the 2D FDTD simulation of GPR inspection, a dry concrete slab, whose width and depth are respectively 1.524 m and 0.762 m, was modeled. A rectangular void artificially embedded at a depth of d was considered as the target to be detected. The thickness of the defect h is taken as 0.762 cm in all simulation cases. The dry concrete is modeled as a lossless dielectric with a dielectric constant (ϵ'_r) of 4, while the dielectric constant of the void (filled with air) is unity ($\epsilon'_0 = 1$). Figure 4 illustrates the computational domain and the concrete structure with a subsurface defect. Two parameters were considered in the FDTD simulation cases; defect depth d and

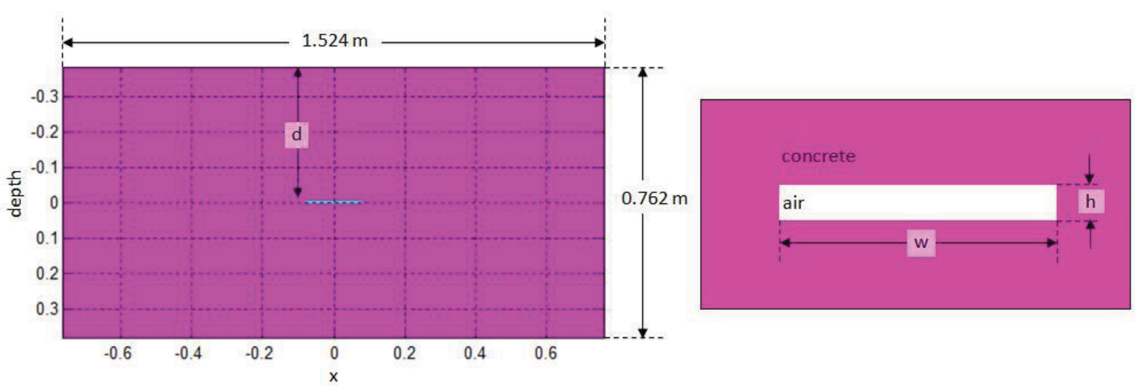

Figure 3. Waveform of the incident GPR signal

defect width w. Thirty-two simulation cases including five defect depths and sixteen defect widths were used. Table 1 lists all the thirty-two defect scenarios.

5. SIMULATION AND IMAGE PROCESSING RESULTS

5.1 Simulated GPR B-scan Images and Image Processing Procedure

A raw GPR B-scan image is shown in Figure 5.1 (A) using the D149W12 (d = 37.846 cm and w = 3.048 cm) concrete slab as an example. A clean GPR response was generated by using an intact concrete slab, and the result is shown in Figure 5.1 (B). Raw GPR images are first processed by removing the background signal (GPR

Table 1. Defect scenarios

Simulation Case	**d (cm)**	**d (Δx)**	**w (cm)**	**w (Δx)**
D149W64	37.846	149	16.256	64
D149W60	37.846	149	15.240	60
D149W56	37.846	149	14.224	56
D149W52	37.846	149	13.208	52
D149W50	37.846	149	12.700	50
D149W48	37.846	149	12.192	48
D149W44	37.846	149	11.176	44
D149W40	37.846	149	10.160	40
D149W36	37.846	149	9.144	36
D149W32	37.846	149	8.128	32
D149W30	37.846	149	7.620	30
D149W28	37.846	149	7.112	28
D149W24	37.846	149	6.096	24
D149W20	37.846	149	5.080	20
D149W16	37.846	149	4.064	16
D149W12	37.846	149	3.048	12
D129W64	32.766	129	16.256	64
D129W48	32.766	129	12.192	48
D129W32	32.766	129	8.128	32
D129W24	32.766	129	6.096	24
D129W16	32.766	129	4.064	16
D129W12	32.766	129	3.048	12
D109W64	27.686	109	16.256	64
D109W48	27.686	109	12.192	48
D109W32	27.686	109	8.128	32
D109W24	27.686	109	6.096	24
D109W16	27.686	109	4.064	16
D109W12	27.686	109	3.048	12
D99W64	25.146	99	16.256	64
D99W12	25.146	99	3.048	12
D89W64	22.606	89	16.256	64
D89W12	22.606	89	3.048	12

image of the concrete slab without defect), resulting in a ridge wave response shown in Figure 5.1 (A). Processed GPR images are then windowed by taking out the center part of the ridge wave response, as shown in Figure 5.1 (B).

The concept of GPR image processing in this approach is to calculate the curvature of the ridge wave in GPR images and relate it to the width of the rectangular defect w. To so do, we need to extract the pattern of the ridge waves in Figure 5.1 for the curvature calculation. Local maximums were taken from the ridge waves and a low-pass filter was applied four times to remove the ripples in the extracted ridge curve. Figure 5.1 (A) shows the extracted ridge curve from Figure 5.1 (B) after the application of low-pass filter four times. Calculation of the curvature of ridge curves is illustrated in Figure 5.1 (B). The curvature index k is defined as the inverse of the radius of curvature; $k = \frac{1}{r}$.

The three-point selection scheme in Figure 5.1 (B) is performed by choosing the peak point (center) and two points (left and right) away from the center at an equal distance of x_d. A parametric study on the value of x_d was performed. It is found that, in the range of $109\Delta x$ and $116\Delta x$, a linear relationship between k and w can be defined. Figure 5.1 shows the linear relationships between k and x_d for sixteen values of w.

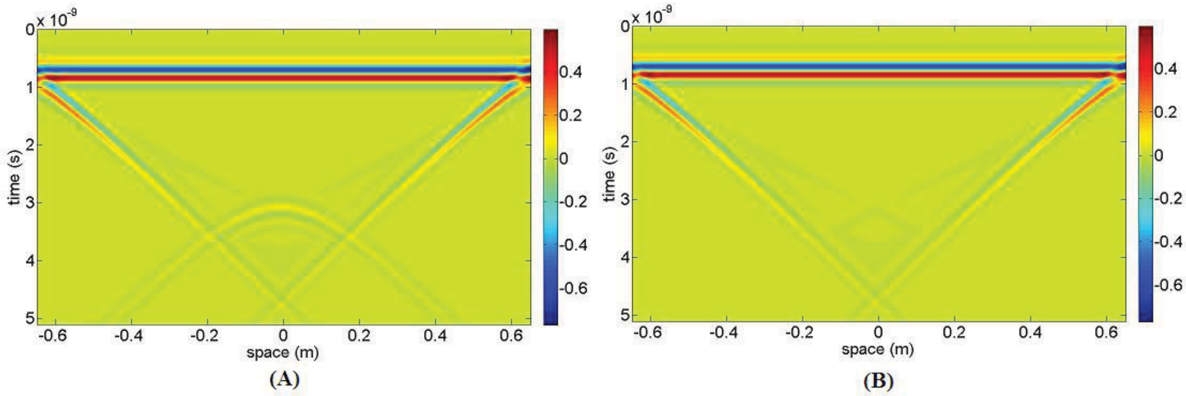

Figure 4. Raw B-scan image of damaged and intact concrete slabs

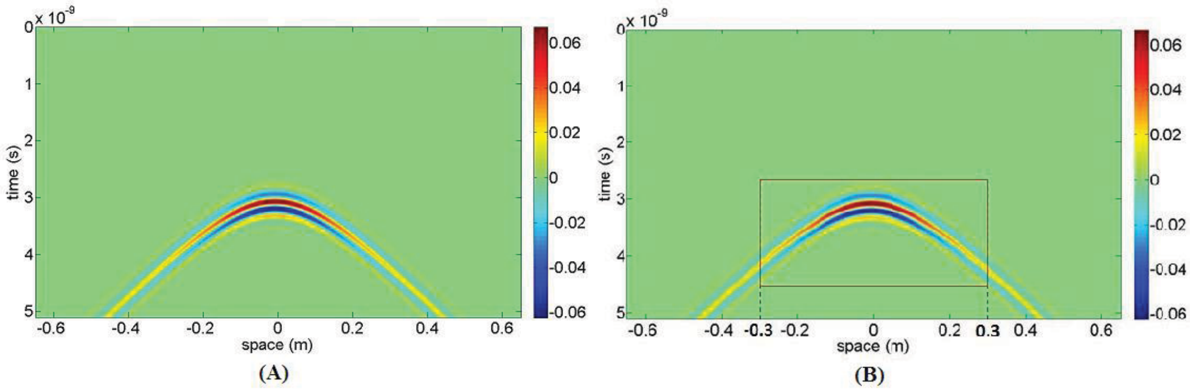

Figure 5. Clean GPR response and the windowed area

5.2 Proposed Quantitative Relationship

In developing the relationship between k and w, x_d was set to be $116\Delta x$ or 30 cm. In the proposed approach, a benchmark case was selected as the basis for case comparison, which is the smallest defect width case ($w_b = 12\Delta x$). A relative defect width is defined by

$$w_r = w - w_b \tag{4}$$

where w_r is the relative defect width and w the actual defect width. Through a series of error analysis in the curve fitting process, two equations are proposed.

$$w_r = A_1\Delta k + A_2 \tag{5}$$

$$w_r = B_1\Delta k^3 + B_2\Delta k^2 + B_3\Delta k + B_4 \tag{6}$$

where A_1 = 2,950, A_2 = 1, B_1 = 3.719×10^8, B_2 = -2.553×10^5, B_3 = 2,825, and B_4 = 1.013. Performance of these two equations is provided in Figures 5 and 6, respectively.

With the above results, we have

$$w = (A_1\Delta k + A_2) + w_b \tag{7}$$

$$w_r = \left(B_1\Delta k^3 + B_2\Delta k^2 + B_3\Delta k + B_4\right) + w_b \tag{8}$$

For example, using 3.5 GHz signal and follow the procedure described above, the crack width is estimated to be xxx (Eq.[7]) and yyy (Eq.[8]) when Δk is zzz.

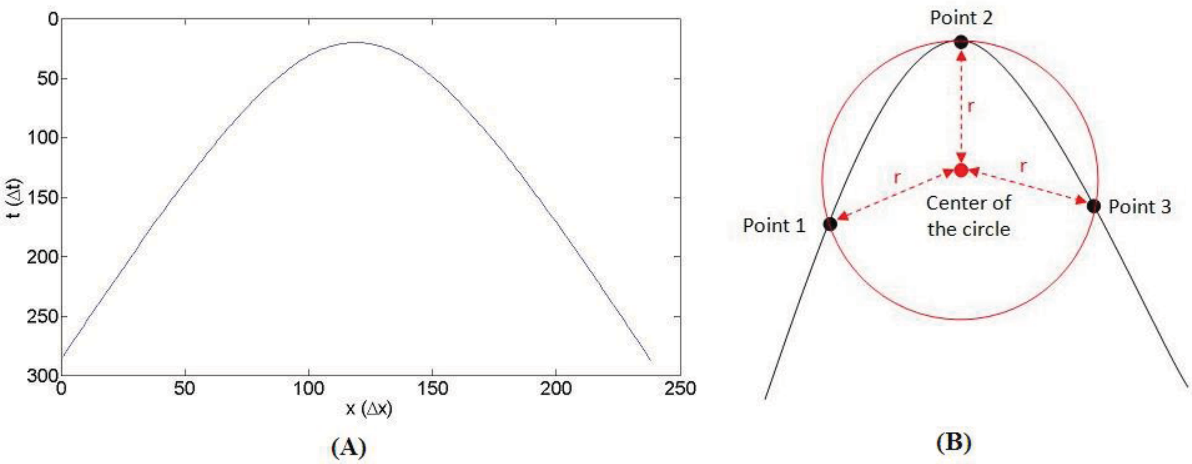

Figure 6. Extracted ridge curve and the curvature calculation scheme

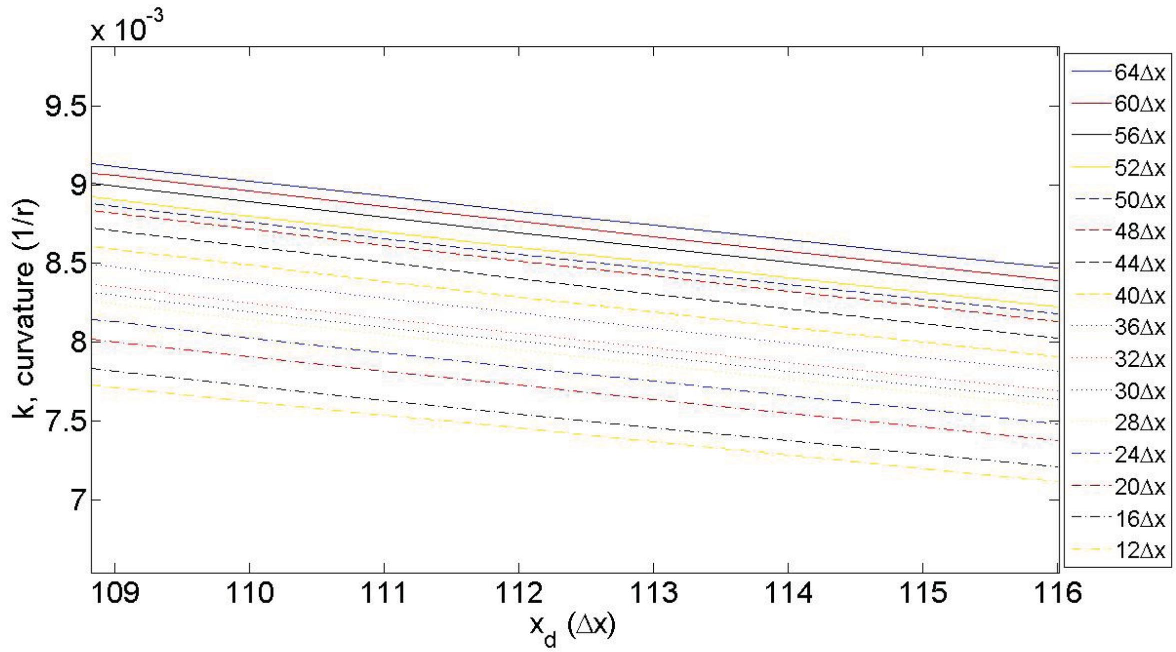

Figure 7. Clean GPR response and the windowed area

6. SUMMARY AND DISCUSSION

In this paper, an approach for the geometric analysis of GPR images to estimate the width of a subsurface rectangular defect in concrete slabs is proposed. Procedure of the geometric analysis is summarized in the following.

- Collection/generation of raw GPR images
- Pre-processing of the raw GPR images – Extracted ridge curves
- Low-pass filtering of extracted ridge curves for the calculation of curvature
- Determination of the reference length (e.g., width, length)
- Curve fitting between the reference length and the curvature

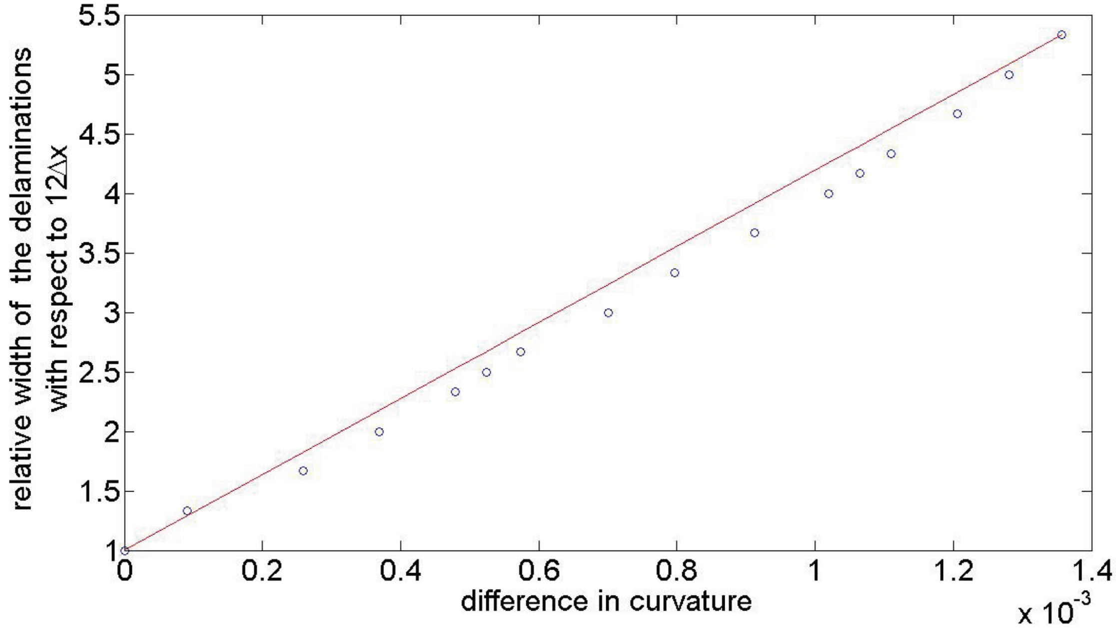

Figure 8. Performance of Eq. [5] – Linear fit

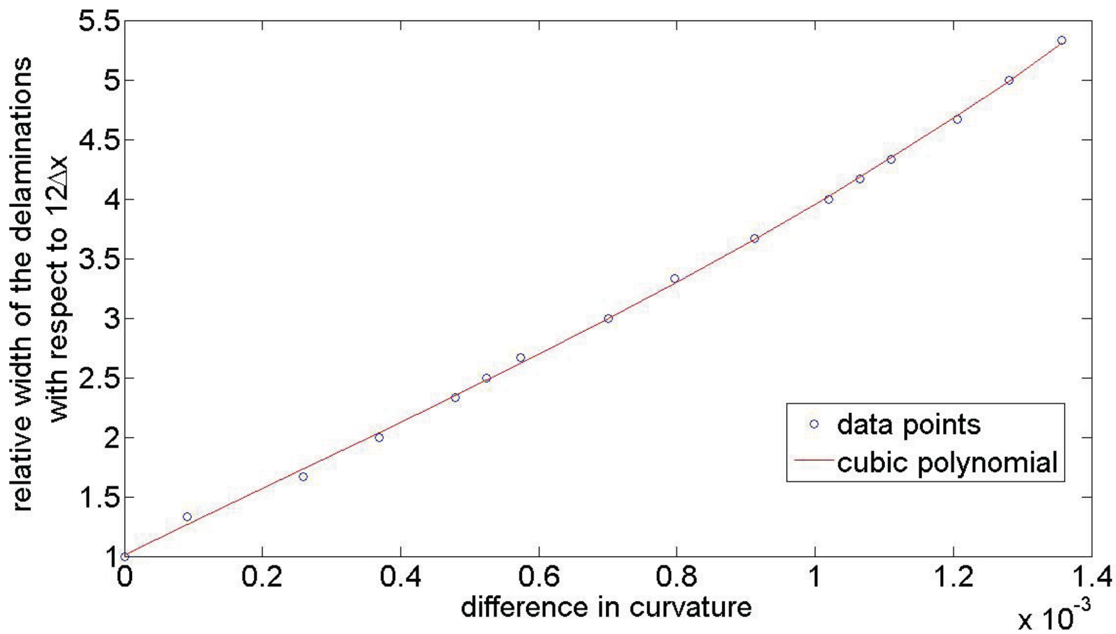

Figure 9. Performance of Eq. [6] – Cubic fit

In the proposed approach, only an ideal crack shape (rectangular) is considered. Also, the GPR scanning/inspection velocity is assumed to be constant. The shape of ridge waves/curves will be different when the inspection velocity changes, although the relationship between the shape of ridge waves/curves and inspection velocity can be linearly derived. Multiple reflections can be expected from anomalies at deeper locations, but signal attenuation also becomes stronger if the subsurface medium is lossy.

While the simulation results were obtained by using a modulated Gaussian signal (center frequency = 3.5 GHz), it is believed the approach can be applied to the analysis using other frequencies.

7. ACKNOWLEDGMENTS

This work was supported by the National Institute of Standards and Technology (NIST) Technology Innovation Program (TIP) through the VOTERS (Versatile Onboard Traffic Embedded Roaming Sensors) project led by Prof. Ming Wang from Northeastern University, Boston, MA. The authors sincerely thank NIST TIP for the financial support.

REFERENCES

[1] D. J. Daniels (ed.), *Ground Penetrating Radar*, Institute of Electrical Engineers, 2nd ed., 2004.

[2] A. Taflove, *Computational Electrodynamics – The Finite-Difference Time-Domain Method*, Artech House, Norwood, MA, 1995.

[3] K. S. Yee, "Numerical solution of initial boundary value problems involving Maxwell's equations in isotropic media," IEEE Trans. Antennas and Propagation, AP-14(3), pp.302-307, 1966.

[4] M. Neyrat, C. Guiffaut, A. Reineix, F. Reynaud, "Fast modelling using fdtd method and wave front inverse method for multisensor GPR simulations in the time domain," *Microwave and Optical Technology Letters*, 51(3), March 2009.

[5] K. Belli, C. Rappaport, H. Zhan, S. W. Fascetti, "Effectiveness of 2-D and 2.5-D FDTD ground-penetrating radar modeling for bridge-deck deterioration evaluated by 3D FDTD," *IEEE Transactions on Geoscience and Remote Sensing*, 47(11), November 2009.

[6] H. Zhan, K. Belli, S. W. Fascetti, C. Rappaport, "Effectiveness of 2d fdtd ground penetrating radar modeling for bridge deck deterioration evaluated by 3D FDTD," *IEEE IGARSS Conference*, 2008.

[7] S. Liu, Z. Zeng, L. Deng, "FDTD simulations for ground penetrating radar in urban applications," *ASCE Journal of Geophysics and Engineering*, 4, pp.262-267, August 2007.

[8] S. Nojavan, F. G. Yuan, "Damage identification using electromagnetic waves based on born imaging algorithm," *ASCE Journal of Engineering Mechanics*, 135(7), pp.717-728, July 2009.

[9] R. W. Hamming, *Digital Filters*, Prentice Hall, 3rd ed., 1989.

[10] K. Courant, K. Friedrichs, H. Lewy, "On the partial difference equations of mathematical physics," *IBM Journal*, pp.215-234, March 1967.

[11] J.-P. Berenger, "Perfectly Matched Layer (PML) for Computational Electromagnetics," Synthesis Lectures on Computational Electromagnetics, 2007.